Journal of Petroleum Science and Engineering 196 (2021) 107742

Contents lists available at ScienceDirect

Journal of Petroleum Science and Engineering

journal homepage: http://www.elsevier.com/locate/petrol

Chemical resistance and mechanical properties of nanosilica addition in oil well cement

Giovanni dos Santos Batista [a], Luana Bottoli Schemmer [a], Tiago de Abreu Siqueira [b], Eleani Maria da Costa [a,*]

[a] School of Technology, Pontifical Catholic University of Rio Grande do Sul, 6681 Ipiranga Avenue, Building 30, Room 111/F, 90619-900, Porto Alegre, RS, Brazil
[b] Institute of Petroleum and Natural Resources, Pontifical Catholic University of Rio Grande do Sul, 6681 Ipiranga Avenue, Building 96J, 90619-900, Porto Alegre, RS, Brazil

ARTICLE INFO

Keywords:
SiO_2 nanoparticles
Oil well cement
CO_2 degradation

ABSTRACT

The aim of this study was to evaluate the chemical resistance and mechanical properties of cement class G with n-SiO_2 addition after being exposed to CO_2-saturated water at HPHT, simulating geological carbon storage condition. Four different amounts of n-SiO_2 (0.5, 1, 1.5 and 3 wt%) and a standard cement (STD Cement) were tested with CO_2-saturated water at 150 bar and 90 °C for 7 and 56 days. The workability of the slurries was evaluated by mini slump test and helium gas pycnometry was used to measure the specific density of unreacted hardened cement systems. Zones affected by CO_2 reactions (bicarbonated, carbonated and portlandite depleted zones) and unreacted core were analyzed using optical and scanning electron microscopes, energy dispersive spectroscopy by line scan, X-ray microtomography and atomic force microscopy. Vickers microhardness and uniaxial compressive strength were used to obtain information about alteration in mechanical properties. The results showed that the addition of n-SiO_2 reduced the workability of the slurries and had insignificant influence on specific density of the hardened cement. After 7 days of exposure to CO_2 medium, the 1.5% n-SiO_2 was the most effective cement system to reduce CO_2 degradation, decreasing the chemical altered thickness to 2.63 mm when compared to STD Cement (3.06 mm). Results from 56 days of exposure to CO_2 show that only 0.5% n-SiO_2 cement system is similar in terms of carbonation to STD Cement. For other n-SiO_2 amounts (1%, 1.5% and 3%) the thicknesses of chemically altered layer are bigger than STD Cement. However, changes in chemical composition, microstructure and density from periphery to the core of the cement system were less accentuated in the cement systems with n-SiO_2 addition after 56 days of cement systems exposure to CO_2. Furthermore, the n-SiO_2 cement systems presented a lower loss in compressive strength values when compared to STD Cement after reaction with CO_2.

1. Introduction

Carbon Capture and Storage (CCS) is one of the most studied methods for greenhouse gas mitigation (Aminu et al., 2017; Anwar et al., 2018; Leung et al., 2014; Yan and Zhang, 2019). This technology may reduce 20% of CO_2 emissions by 2050 and limit the increase of average global temperature to 2 °C (Aminu et al., 2017; Leung et al., 2014). The main objectives of CCS are to capture, transport and inject CO_2 in saline aquifers, coal beds and depleted oil wells (Bai et al., 2015; Barlet-Gouédard et al., 2009). The Enhanced Oil Recovery (EOR) and Enhanced Coal Bed Methane (ECBM) processes involve CO_2 injection, a significant catalysts step in CCS development (Lake et al., 2019; Leung et al., 2014). The last and most challenging stage of CCS is the CO_2 confinement, which must guarantee minimum CO_2 leakage rates. High CO_2 leakage rates increase the risk of fresh water contamination and may cause several problems to vegetation, animals, people and the whole environment (Abid et al., 2015; Zhang and Bachu, 2011). Since the leakage may occur through the well cement, it is important to ensure that the well cement is leak-tight. The CO_2 is injected into the well above its critical point (73.8 bar and 31.1 °C) and stored in reservoirs usually at depths more than 800 m. In this condition the CO_2 has high density, high diffusivity and higher chemical reactivity. However, the class G and class H oil well cements are unstable in CO_2-rich environments. The hardened cement paste reacts with carbonic acid and experiences severe

* Corresponding author.
E-mail address: eleani@pucrs.br (E.M. Costa).

https://doi.org/10.1016/j.petrol.2020.107742
Received 28 January 2020; Received in revised form 31 July 2020; Accepted 4 August 2020
Available online 16 August 2020

chemical changes that compromise mechanical properties and affect its durability after long CO_2 exposure times (Abid et al., 2015; Bagheri et al., 2018; Bai et al., 2016; Barlet-Gouédard et al., 2007; Bertos et al., 2004; Bjørge et al., 2019; Carey et al., 2010; Huet et al., 2011; Kutchko et al., 2009, 2008; Lesti et al., 2013; Matteo et al., 2018; Omosebi et al., 2016; Yang et al., 2016; Zhang and Talman, 2014). Therefore, one of the major issues of CCS technology applying might be to avoid or minimize the chemical interaction between supercritical CO_2 and cement, which may lead to cement sheath partial or total loss, creating potential leakages paths during and after CO_2 injection stages.

The Portland cement is fundamentally composed by clinker, which contains tricalcium silicate (C_3S), dicalcium silicate (C_2S), tricalcium aluminate (C_3A) and tetracalcium aluminoferrite (C_4AF) (Bentz, 1997; Taylor, 1990). The hydration process occurs in the presence of water. C_3S and C_2S produce hydrated calcium silicate (C–S–H) and calcium hydroxide ($Ca(OH)_2$, portlandite) (Nelson and Guillot, 2006; Taylor, 1990). Equations (1) and (2) express the main chemical reactions in the cement hydration process.

$$2C_3S + 6H_2O \rightarrow C-S-H + 3Ca(OH)_2 \quad (1)$$

$$2C_2S + 4H_2O \rightarrow C-S-H + 3Ca(OH)_2 \quad (2)$$

The process of C_3A and C_4AF hydration is slower due to the presence of gypsum. This component causes the formation of more portlandite and ettringite (AFt), responsible for thickening time (Equations (3) and (4)) (Mehta and Monteiro, 2013; Nawy, 2008; Taylor, 1990). Non-hydrated grains are also present.

$$C_3A + C\bar{S}.2H_2O + 26H_2O \rightarrow AFt \quad (3)$$

$$C_4AF + 3C\bar{S}.2H_2O + 30H_2O \rightarrow AFt + Ca(OH)_2 + FH_3 \quad (4)$$

The cement degradation process that occurs in the presence of CO_2 is divided in three stages: Firstly, the CO_2 dissolves in water to form carbonate (CO_3^{2-}) and bicarbonate (HCO_3^-) ions. These ions react with Ca $(OH)_2$ and C–S–H, producing a high porosity region (dissolution zone). The second stage is the precipitation of calcium carbonate ($CaCO_3$), which creates a dense zone with high hardness known as carbonated zone. The pH reduction caused by the consumption of alkaline phases leads to the third stage, which is the dissolution of the precipitated $CaCO_3$. This process creates a high porosity zone known as bicarbonated zone (Bagheri et al., 2018; Barlet-Gouédard et al., 2007; Huet et al., 2011; Kutchko et al., 2009, 2008). Equations (5)–(7) represent the first stage. Equations (8)–(11) represent the second stage. Equations (12) and (13) represent the last stage of cement degradation process.

$$CO_{2(aq)} + H_2O \rightarrow H_2CO_{3(aq)} \quad (5)$$

$$H_2CO_{3(aq)} \rightarrow H^+_{(aq)} + HCO^-_{3(aq)} \quad (6)$$

$$HCO^-_{3(aq)} \rightarrow H^-_{(aq)} + CO^{2-}_3 \quad (7)$$

$$Ca(OH)_{2(s)} + 2H^+ + CO^{2-}_3 \rightarrow CaCO_{3(s)} + 2H_2O \quad (8)$$

$$C-S-H_{(s)} + 2H^+ + CO^{2-}_3 \rightarrow CaCO_{3(s)} + SiO_x(OH)_x \quad (9)$$

$$Ca(OH)_{2(s)} + H^+ + HCO^-_3 \rightarrow CaCO_{3(s)} + 2H_2O \quad (10)$$

$$C-S-H_{(s)} + H^+ + HCO^-_3 \rightarrow CaCO_{3(s)} + SiO_x(OH)_x \quad (11)$$

$$CO_2 + H_2O + CaCO_{3(s)} \rightarrow Ca^{2+} + 2HCO^-_3 \quad (12)$$

$$2H^+ + CaCO_{3(s)} \rightarrow CO_2 + Ca^{2+} + H_2O \quad (13)$$

The carbonation process is directly related to Gibbs free energy. Low energy values result in deep carbonation. Energy values increase as the Ca/Si ratio decreases. High production of C–S–H results in low $Ca(OH)_2$ quantity, which increases the chemical resistance of the paste (Duguid et al., 2011; Yang et al., 2016). Table 1 presents Gibbs free energy values in different temperatures between CO_2 and main hydration products of cement paste.

Table 1
Gibbs free energy between CO_2 and cement hydrated compounds (Yang et al., 2016).

Hydration products	ΔG^0_T 25 °C (KJ.mol^{-1})	ΔG^0_T 60 °C (KJ.mol^{-1})	ΔG^0_T 85 °C (KJ.mol^{-1})	ΔG^0_T 127 °C (KJ.mol^{-1})
C_3S	−147.75	−128.67	−112.41	−70.78
$C_3S_2H_3$	−72.88	−70.06	−68.23	–
$Ca(OH)_2$	−38.19	−39.16	−38.76	−39.06
C_2S	−35.14	−29.63	−26.03	−20.26
$C_2SH_{1.17}$	−30.72	−0.19	−12.45	−20.09
$C_5S_6H_{5.5}$	74.32	80.94	89.77	103.76
C_6S_6H	104.59	113.72	137.52	178.39

One of the alternatives to increase Gibbs free energy and consequently minimize cement carbonation is to incorporate pozzolanic material to decrease Ca/Si ratio. When incorporating this material, a secondary C–S–H is formed, and a longer C–S–H chain is produced. Furthermore, the porosity is reduced and the mechanical strength of the hardened paste is increased (El-Diadamony et al., 2018; Shao et al., 2019; Wang and Ishida, 2019; Xiao et al., 2019). Some studies about the addition of pozzolans to minimize the cement paste degradation in wells for geological carbon storage have been conducted with limited success when tested under reservoir conditions (Abid et al., 2015; Barlet-Gouédard et al., 2007; Huet et al., 2011; Kutchko et al., 2009; Ledesma et al., 2020; Soares et al., 2015; Zhang et al., 2014, 2013). Employing nanoparticles could be another important solution to reinforce the cement to operate in these critical conditions that involve high pressure and high temperature (HPHT). This is because many studies have demonstrated that the use of pozzolanic material in nanometric scale accelerates hydration reactions and promotes better functionalities to cement-based materials due to its low particle size and high surface area (Ershadi et al., 2011; Santra et al., 2012). Nanosilica (n-SiO_2) has been used in many civil industry studies mainly because its low cost when compared to other nanoparticles, besides presenting relatively high pozzolanic activity and acting as a nanofiller. This material densifies the matrix, enhances cement mechanical strength and increases durability of cement-based materials (Marshdi, 2018; Senff et al., 2009). The n-SiO_2 can also enhance viscosity and reduce cement thickening time and fluid loss (Ershadi et al., 2011; Santra et al., 2012). However, there have been a very limited discussions on n-SiO_2 application potential in the oil and gas industries, especially for use in CO_2 sequestration sites. Most of studies for n-SiO_2 application in oil and gas fields are concentrated on the slurry rheology and mechanical resistance investigation (Bu et al., 2018; El-Gamal et al., 2017; Hu et al., 2019; Huet et al., 2011; Janković et al., 2016; Liu et al., 2018; Rostami et al., 2019; Wang and Ishida, 2019). But scarcely research has been conducted evaluating chemical resistance in CO_2-rich environments under CCS condition. Griffin et al. (2013) studied the significance of n-SiO_2 (1% and 3% in wt.) on oil well cement degradation in carbonated brine environment, but realized the degradation tests at atmospheric pressure in a glass reactor vessel at 50 °C. Jeong et al. (2018) replaced cement class G by colloidal n-SiO_2 and performed degradation tests in CO_2-brine solution at a pressure of 100 bar and 40 °C, but tested only one n-SiO_2 amount (2 wt%). Both studies showed that cement paste combined with n-SiO_2 had a better performance in CO_2 presence, as consequence of matrix densification promoted by n-SiO_2 addition. In the best of our knowledge, the Jeong et al. (2018) is the only published study that performed CO_2 degradation tests using n-SiO_2 in oil well cement in autoclave at temperature and pressure characteristics of carbon geological storage sites. However, degradation of oil well cement in CO_2 presence is a complex process that is affected by many interacting factors including the cement paste porosity, existence of additives, the degree of hydration prior to

Table 2
n-SiO_2 and cement properties.

Material	Particle size	Density (g. cm^{-3})	Solid/ water ratio (%)	pH	BET surface area (m^2. g^{-1})
n-SiO_2	50 nm	1.495	58.5	9.5–10.5	35.29
Cement Class G	7.3 μm	2.80–3.20	Powder	12–14	0.82

degradation tests, pressure, temperature, etc. Therefore, there is need of more experimental studies that evaluate the n-SiO_2 reinforced cement degradation conducted in HPHT autoclave simulating carbon geological reservoir conditions. Another significant aspect, is the necessity of testing different n-SiO_2 amounts, since most of the studies using nanoparticles have indicated the existence of an optimum amount to be added that enhances chemical and mechanical properties (El-Gamal et al., 2017; Flores et al., 2017; Liu et al., 2018; Thakkar et al., 2019).

In this context, in this study cement class G with different n-SiO_2 amounts (0, 1, 1.5 and 3 wt%) were submitted to CO_2 degradation tests at HPHT, simulating an oil well for geological carbon storage of about 1,500 m. Chemical resistance to CO_2 attack and mechanical properties were evaluated by multiple characterization methods application in order to better understand the role of n-SiO_2 in oil well cement for CCS utilizations.

2. Materials and methods

2.1. Materials

The API class G oil well Portland cement used in this study was supplied by Lafarge Holcim Brasil S.A. The nanosilica (n-SiO_2) was acquired from Akasel. The properties of these materials are shown in Table 2. The n-SiO_2 X-ray diffractogram is presented in Fig. 1 and shows the characteristic peak of SiO_2.

The amounts of cement replacement by n-SiO_2 in the cement systems were 0.5, 1, 1.5 and 3% by weight. A cement slurry without any additives (STD Cement) was prepared to better understand the n-SiO_2 effect on the chemical and mechanical properties.

2.2. Preparation of cement slurries and test specimens

The cement slurry was prepared according to the 10 A specification of the American Petroleum Institute (API, 2009). Due to the large surface area of n-SiO_2, the rheology of the cement slurry is affected. Thus, instead of using a water/binder ratio, a water/solids ratio of 0.44 for all systems was used. Table 3 shows the formulations of the cement slurries. The n-SiO_2 was mixed with water for 5 min before applying the 10 A specification. As described in the 10 A specification, the mixer has been set up to a rotation of 4,000 rpm for 15 s for the cement addition and then to 12,000 rpm for 35 s. For each degradation test, a new cement slurry was made.

The mini slump test proposed by Kantro and adopted by Collins et al. (2012) was used to verify the workability of the cement paste. Six measurements of the spread diameter were performed, and the arithmetic average was used to represent the results.

A polymeric cylindrical mold of 43.2 mm height and 21.6 mm diameter was used to produce the specimens. Then, the specimens were cured in an autoclave inside a pressure vessel filled with water and nitrogen (N_2) pressure of 60 bar and temperature of 60 °C for 8 h, a similar condition to an oil well before the CO_2 injection. These cure conditions produce more than 70% of reaction products and further hydration of cement is slow (Pang et al., 2013). Also, curing 24 h under autoclave is equivalent to 28 days of atmospheric curing (Kołakowski et al., 1994). The matrix also suffers less drying shrinkage, no efflorescence and more resistance against sulfate attacks (Alawad et al., 2015; Neville, 2018).

Helium gas pycnometry was used to compare the cured cement systems specific density to provide information about the filler and pozzolanic effects caused by n-SiO_2 in the microstructure, once it can reduce the pore volume producing a more compact cementitious matrix. The pycnometry analyses were performed on cured cement cylindrical specimens (43.2 × 21.6 mm). For the analyses, the hardened cement samples were oven-dried at 60 °C for 7 days in order to remove humidity and avoid any shrinkage cracks.

2.3. Degradation tests in CO_2 environment

Five specimens were used for each cement system and placed inside a stainless-steel high-pressure vessel of 1 L (AISI 316), half-filled with Milli-Q water, covering all samples, as illustrated in Fig. 2. Milli-Q is an

Table 3
Cement systems composition.

Cement Systems	Cement (g)	Water (mL)	n-SiO_2 solution (g)
STD Cement	600.00	264.00	0.00
0.5% n-SiO_2	597.00	260.41	7.67
1% n-SiO_2	594.00	256.82	15.33
1.5% n-SiO_2	591.00	253.23	23.00
3% n-SiO_2	582.00	242.46	46.00

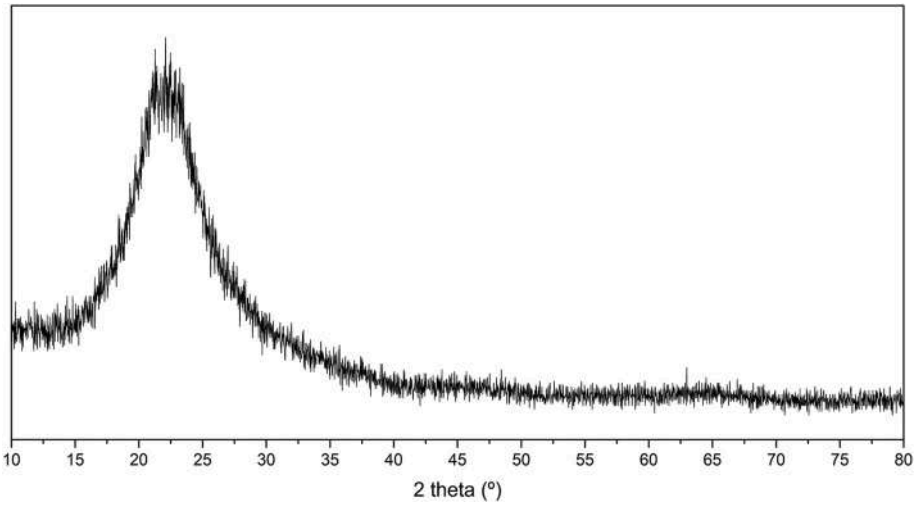

Fig. 1. n-SiO_2 diffractogram, showing the characteristic peak of SiO_2.

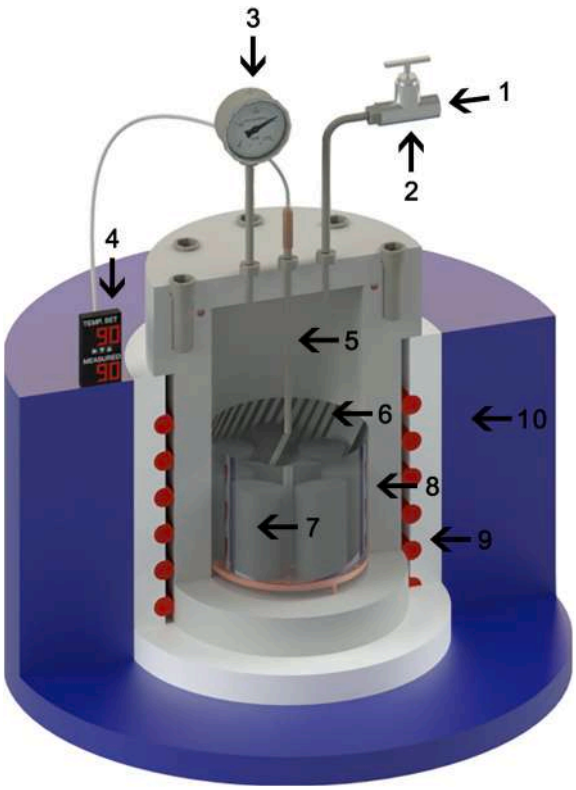

Fig. 2. Pressure vessel model used to simulate an oil well. 1) CO_2 injection; 2) Valve; 3) Manometer; 4) Temperature controller; 5) Thermocouple; 6) CO_2-saturated water; 7) Samples; 8) Pressure vessel; 9) Heating blanket; 10) Heating blanket protection.

ultrapure water that was obtained by using a Direct Water Purification System from Merck.

The pressure and temperature in the chemical degradation tests was set to 150 bar and 90 °C respectively. 99.9% purity CO_2 was used for pressurization. According to van der Meer (2005), the CO_2 reaches the supercritical state in depths between 800 and 850 m and the wellbore pressure presents a gradient of variation of approximately 100 bar. km^{-1}. In this study, the pressure corresponds to a wellbore about 1,500 m depth. The pressure and temperature used for the degradation tests were both above the critical point of CO_2 (73.8 bar and 31.1 °C), appropriate conditions for carbon geological storage. The degradation tests were performed in CO_2-saturated water for 7 and 56 days. The experiments were conducted under static conditions as a simulation of a well distant from the injector or when the CO_2 injection period is finished. When the degradation times were reached, the pressure from the vessel was slowly released.

2.4. Characterization methods

Scanning Electron Microscopy by Field Emission Gun (SEM/FEG-Inspect F50 model, FEI) and Energy Dispersive Spectroscopy (EDS) were used to analyze the cement paste microstructural changes. The samples were cut in 3 mm width discs using a diamond precision saw, ground with SiC sandpaper from #320 to #1200 and polished with alumina 1 μm and 0.3 μm, respectively. The samples were covered with a thin gold film to become conductive. The images were acquired by secondary electron mode to observe the interface between the carbonated zone and the intact core and the Ca/Si ratio from the edge to the core by using EDS line scan.

Computed microtomography (Bruker microCT SkyScan1173) with 130 kV, 61 mA and resolution of 12 μm was used to evaluate the differences in density of the cement paste zones with and without n-SiO_2 addition after CO_2 exposure.

AFM besides generating 3D topographic images with atomic resolution, offers the possibility of surface height and roughness direct measurement associated to materials heterogeneities. Therefore, AFM was used to analyze and compare roughness related to different carbonation fronts in cement systems with and without n-SiO_2. The AFM roughness test enables microstructure uniformity and heterogeneity analysis between these fronts. In general, a more uniform and denser microstructure (lower roughness value) should relate to a cement paste with higher mechanical properties and lower permeability. The Bruker Dimension Icon TP equipment of Atomic Force Microscopy (AFM) with a cantilever probe with nominal thickness of 6.25 μm, resonant frequency of 525 kHz and Spring constant of 200 N/m was used to analyze and compare roughness related to different carbonation fronts from STD cement and 3% n-SiO_2. The scanned areas corresponding to interfacial region were determined by a first analysis with AFM optical microscopy system. The test area was set as 60 μm × 60 μm.

A Vickers Shimadzu HMV-G durometer was used to evaluate $CaCO_3$ precipitation effects on microhardness. The microhardness was measured by applying a 50 g load for 15 s, and measurements were performed with 80 μm step to obtain the hardness transversal profile from bicarbonated zone towards unreacted core.

Compressive strength tests were performed using samples in

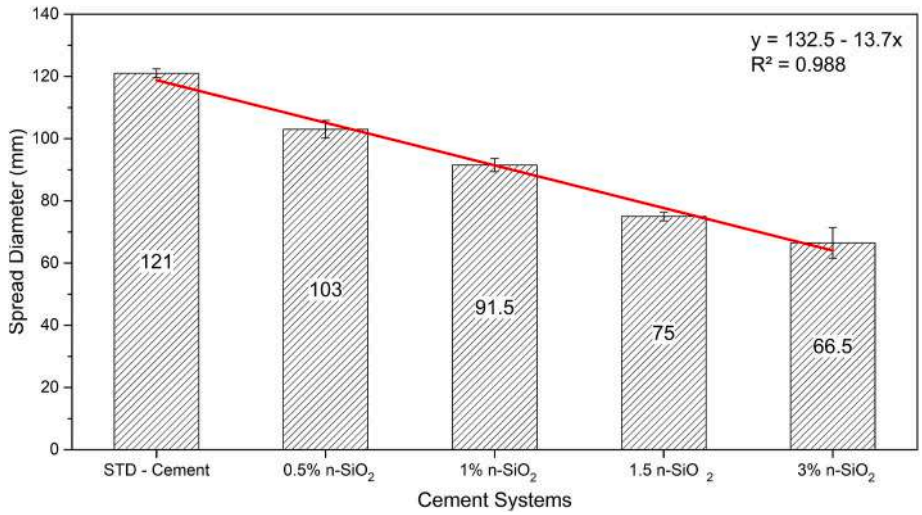

Fig. 3. Cement slurry workability.

Table 4
Hardened cement systems specific densities.

Cement Systems	Specific density ($g.cm^{-3}$)
STD Cement	2.139
0.5% n-SiO_2	2.110
1% n-SiO_2	2.169
1.5% n-SiO_2	2.101
3% n-SiO_2	2.127

triplicate with a speed of 0.1 mm/min in a Shimadzu EMIC, PC200I model to evaluate cement paste mechanical behavior before and after CO_2 degradation. For comparison purpose and reliability on results, cylindrical specimens (43.2 × 21.6 mm) with same age were used in all compressive strength tests.

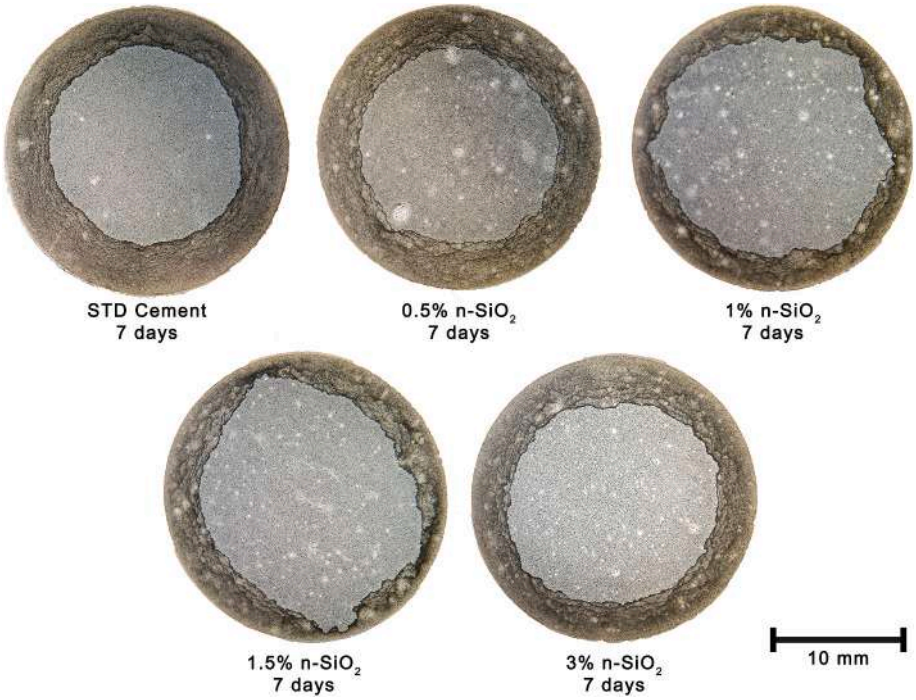

Fig. 4. Cement system transversal sections after being exposed to CO_2-saturated water for 7 days.

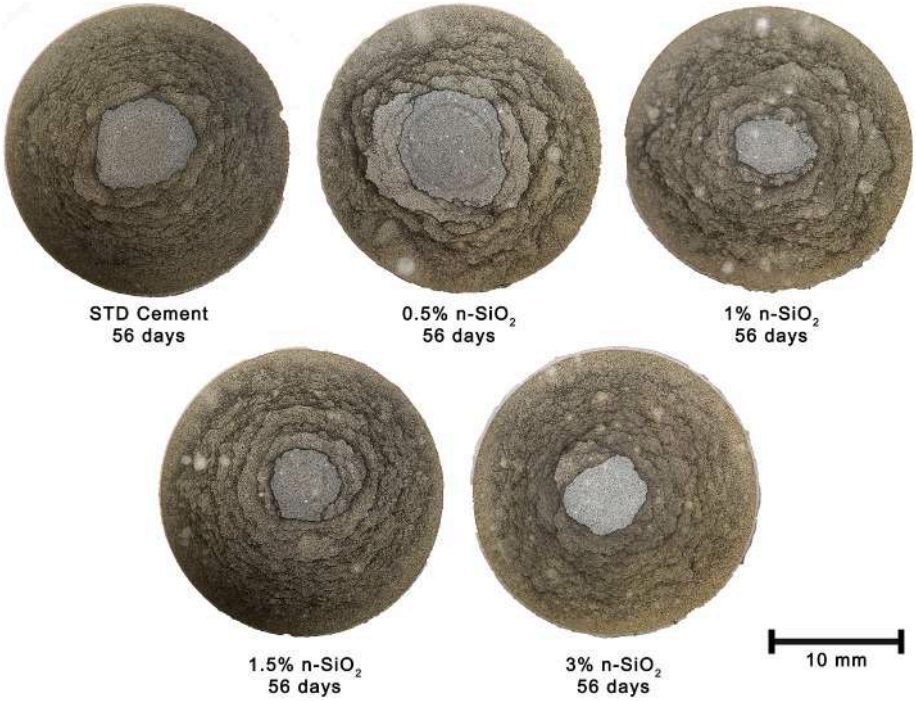

Fig. 5. Cement system transversal sections after being exposed to CO_2-saturated water for 56 days.

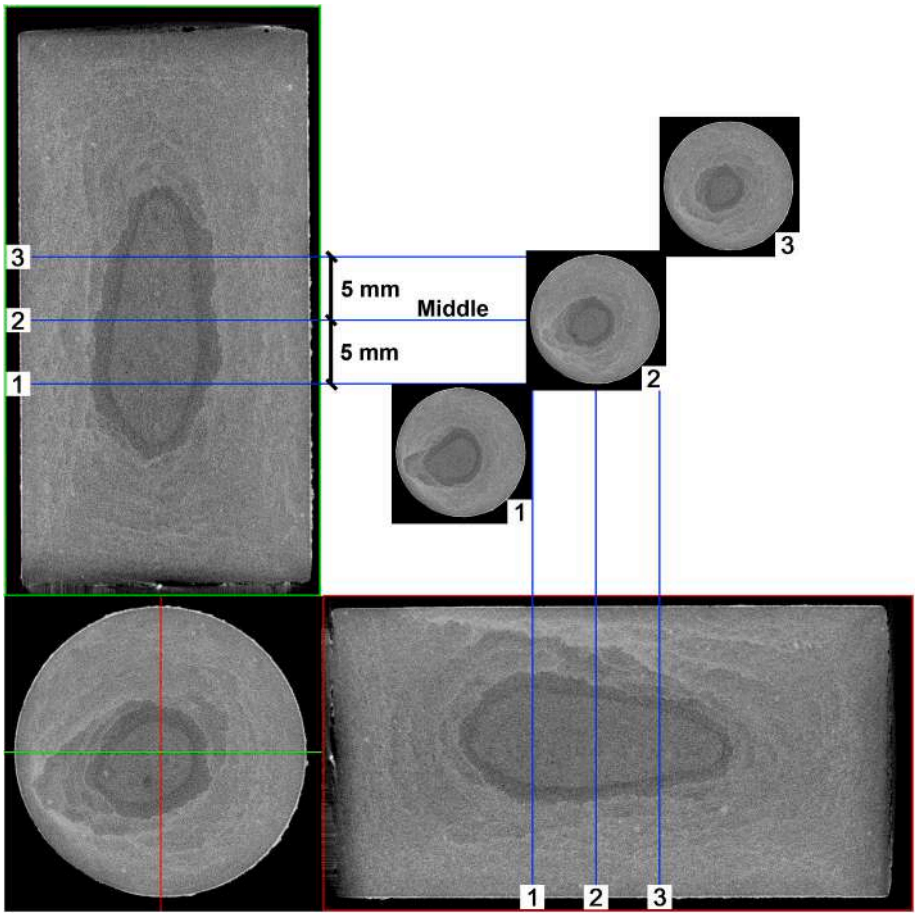

Fig. 6. STD Cement microtomography used for chemically altered thickness measurement. The red and green lines represent longitudinal sections, while the blue lines represent the three transversal sections. (For interpretation of the references to colour in this figure legend, the reader is referred to the Web version of this article.)

3. Results and discussion

3.1. Cement paste workability and density of cement systems

The workability tests were performed right after the mixing in order to investigate the slurry behavior in the presence of n-SiO_2. Fig. 3 demonstrates the spreading diameter for all cement systems. Workability reduces linearly as the n-SiO_2 increases. The spread diameter reduction is possibly related to the n-SiO_2 high specific surface area due to its small particle size. Thus, when the cement is substituted by n-SiO_2, the n-SiO_2 has elevate reaction capacity because of its high specific surface area and a large number of unsaturated bonds, which makes it easier to attract surrounding water molecules to form chemical bonds (Zhuang and Chen, 2019). Therefore, as it absorbs more water, the spread diameter of cement system is reduced. This effect was also observed by Lavergne et al. (2019), by adding of 1.5 wt% of n-SiO_2 caused a spread diameter reduction from 280 mm to 105 mm (decreasing of 62.5%) for a w/c ratio of 0.45. In this study, a lower decreasing (38%) on spread diameter by adding 1.5 wt% of n-SiO_2 was obtained, changing the spread diameter from 121 mm to 75 mm. This difference might be related with higher specific surface area of the n-SiO_2 used by Lavergne et al. (2019).

The reduction on workability is also an evidence that n-SiO_2 behaves not only as a filler to improve microstructure, but also as an activator to promote pozzolanic reaction, shortening hydration period and reaching an early heat of hydration as also observed by Lavergne et al. (2019), Murthy et al. (2019) and Paul et al. (2018).

Table 4 shows cement systems specific densities obtained by gas pycnometry and it is observed that there is no significative variation on this property when n-SiO_2 is added. This is mainly because the cement quantity replaced by n-SiO_2 was very small. Furthermore, as the n-SiO_2 has lower density than cement a decreasing on density is expected with increasing amount of n-SiO_2, but this effect was not observed. This can be an indicative that n-SiO_2 particles can reduce the pore volume, producing a more compact cementitious matrix due their nanofiller and pozzolanic effects. Additionally, the slurry workability reduction and air entrapment observed with n-SiO_2 increasing did not negatively impact the specific density of hardened cement specimens.

3.2. Carbonation behavior

Images obtained by optical microscopy (Figs. 4 and 5) illustrate the chemically altered layer pattern of cement systems after being exposed to CO_2-saturated water for 7 and 56 days at 150 bar and 90 °C, respectively. Various carbonation fronts formed in all cement systems by the degradation process advance towards the cement core as the exposure time increases. However, the number of fronts is inferior and the fronts are thicker in the n-SiO_2 presence probably influenced by the pozzolanic effect, that reduces the portlandite crystal size and amount.

The thicknesses of chemically altered layer caused by the CO_2 attack were obtained from microtomography images. Fig. 6 illustrate the carbonation profile along longitudinal and transversal axes. As the carbonation pattern is not homogeneous, the entire transversal degraded area was considered to measure carbonation thickness. For that purpose, three transversal sections from microtomography were used to obtain the degraded area and then the carbonation thickness

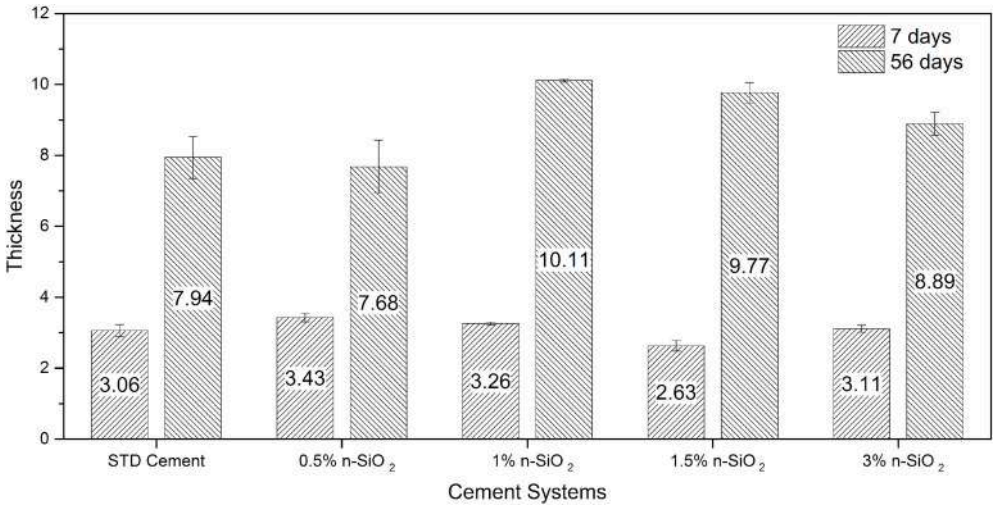

Fig. 7. Chemically altered layer thickness after being exposed to CO_2-saturated water for 7 and 56 days.

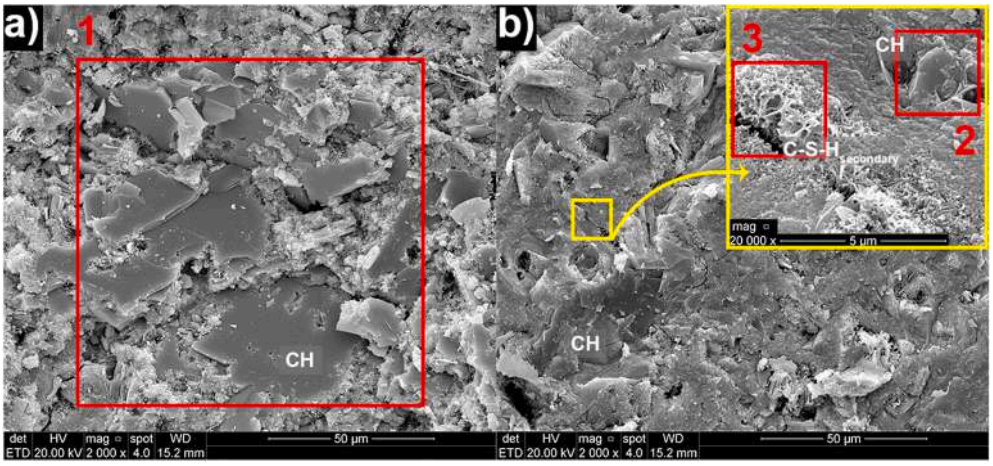

Fig. 8. Unaltered core of (a) STD Cement and (b) 3% n-SiO_2 systems where the yellow square represents an amplification from figure b and area 1 and area 2 are related to portlandite and area 3 is related to secondary C–S–H modification. (For interpretation of the references to colour in this figure legend, the reader is referred to the Web version of this article.)

average and standard deviation values by means of interpolation for all cement systems. The first transversal section was taken exactly at the middle of the specimen, and the other two sections were obtained from 5 mm above and 5 mm below of central line, as shown in Fig. 6.

Fig. 7 shows the chemically altered layer thicknesses for all cement systems after being exposed to CO_2-saturated water for 7 and 56 days. After being exposed to CO_2 for 7 days, the cement systems with n-SiO_2 addition performed similar to the STD Cement in terms of chemical resistance. However, the lowest thickness value was found with 1.5% of n-SiO_2 (2.63 mm), being 16% less profound than the system without addition (3.06 mm). Results from 56 days of exposure to CO_2 show that only 0.5% n-SiO_2 system are similar to STD Cement in terms of carbonation, whereas for other n-SiO_2 amounts (1%, 1.5% and 3%) the chemically altered layer thicknesses are bigger. The n-SiO_2 pozzolanic character induces more C–S–H formation because of the calcium hydroxide consumption by pozzolanic reactions. Thus, as the matrix alkaline reserve and pore solution is reduced it may facilitate the carbonation front advance in cement systems with n-SiO_2.

To better understand the influence of n-SiO_2 in cement microstructure, SEM analysis was used to compare portlandite crystals size and features of unreacted core from STD Cement with n-SiO_2 system. Fig. 8 presents the cement core from both cement systems, STD Cement and 3% n-SiO_2 system, evidencing that both the size and the amount of portlandite crystals reduces significatively (areas 1 and 2 of Fig. 8) when n-SiO_2 is added due to nucleation rate increase and pozzolanic reactions. This effect was observed in all n-SiO_2 systems. The nanomaterial addition also modifies secondary C–S–H structure (area 3 of Fig. 8), filling sub micrometer pores and cracks, acting as an *in situ* fiber reinforcement. The modification in secondary C–S–H structure was also observed by Feng et al. (2013) adding TiO_2 nanoparticles in Portland cement paste.

The n-SiO_2 influence on the carbonation fronts properties were investigated by SEM/EDS, AFM and microhardness. Figs. 9 and 10 show SEM images from cross sections of reacted cement systems after being exposed to CO_2-saturated water for 7 and 56 days at 150 bar and 90 °C. The images on the right are an amplification of the marked areas, where the red line represents the transition between carbonated zone and unreacted core. All cement systems showed a high-density carbonated zone followed by a porous zone, indicating that the reaction mechanism is same that has been reported in literature for cement degradation in a CO_2 rich environment (Abid et al., 2015; Barlet-Gouédard et al., 2007; Huet et al., 2011; Kutchko et al., 2007; Ledesma et al., 2020). The formation of a high porosity degraded zone is due to portlandite consumption and calcium leaching from matrix to solution to form amorphous SiO_2, evident in early degradation time (Fig. 8). The major transport mechanism into the cement is radial diffusion, usually respecting the Fick's second law, where carbonation depth increases

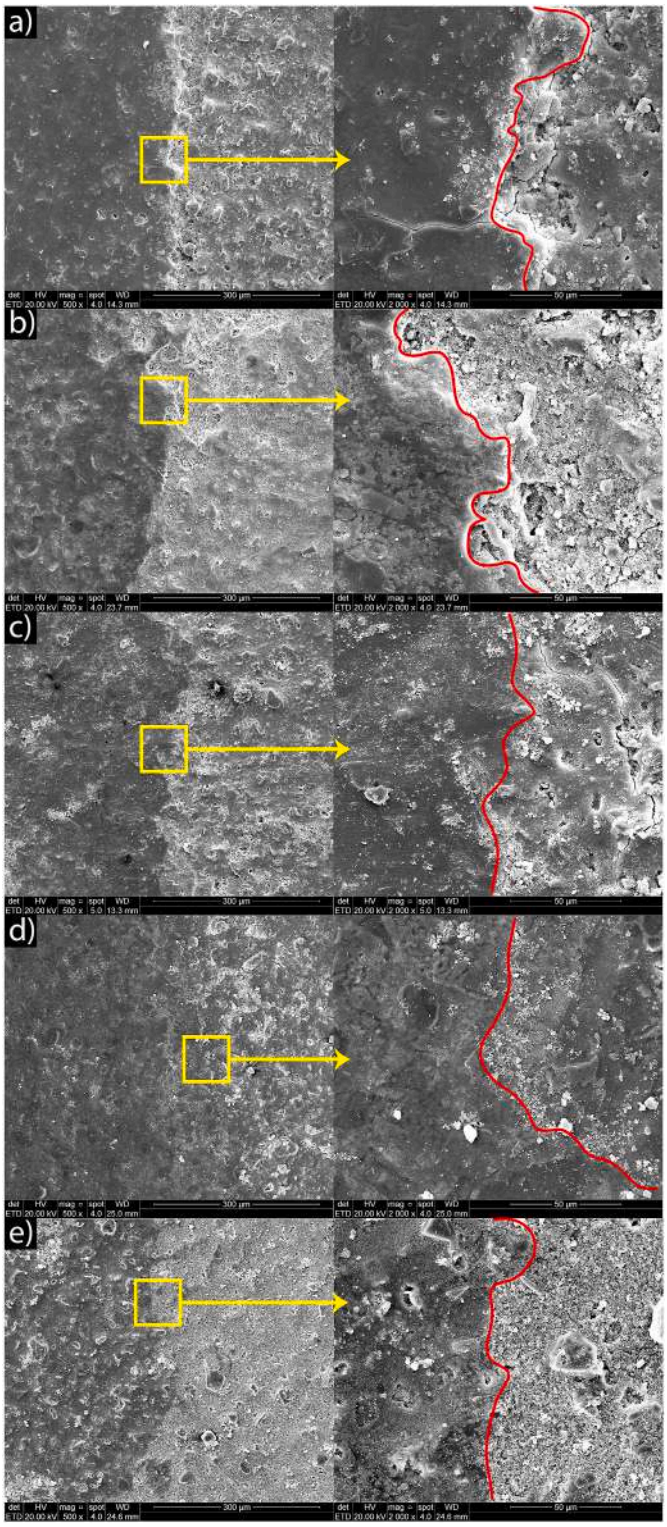

Fig. 9. Cement systems interface between carbonated zone and unaltered core of (a) STD Cement, (b) 0.5% n-SiO_2, (c) 1% n-SiO_2, (d) 1.5% n-SiO_2 and (e) 3% n-SiO_2 after being exposed to CO_2 saturated water for 7 days.

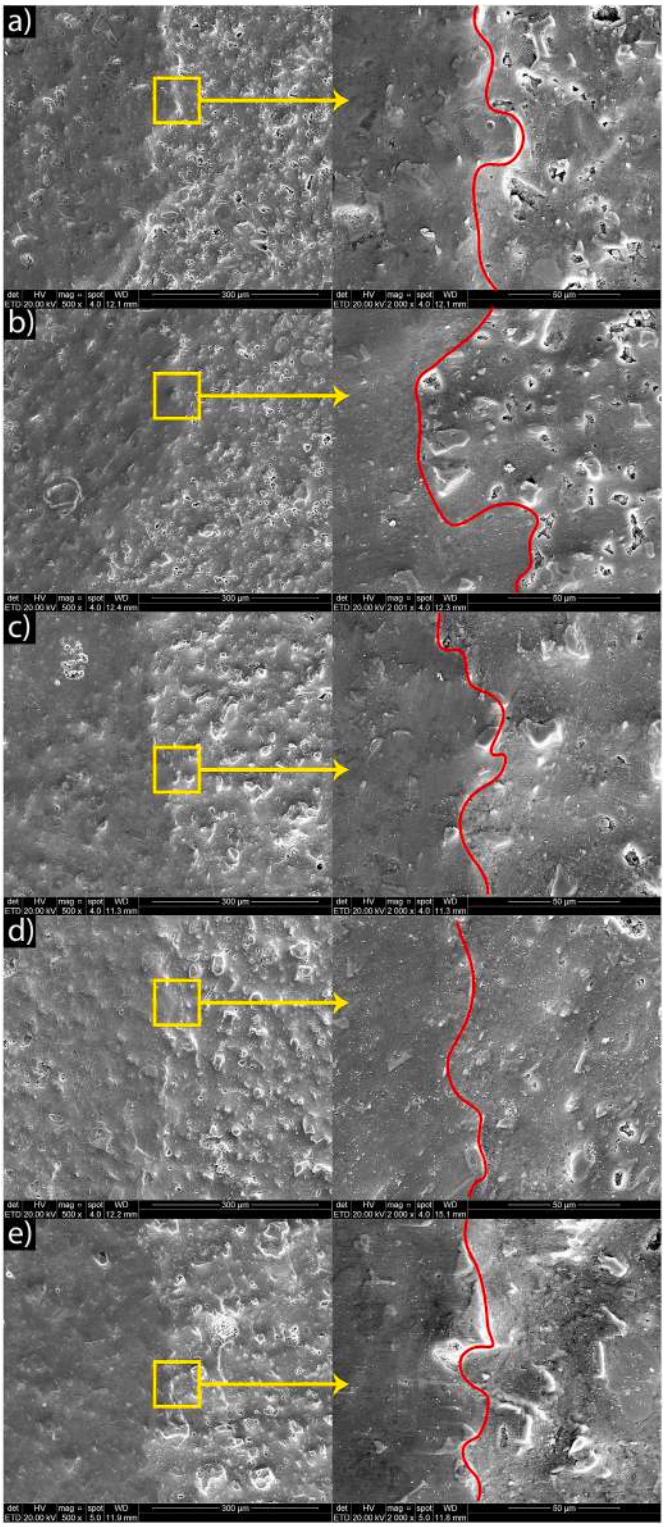

Fig. 10. Cement systems interface between carbonated zone and unaltered core of (a) STD Cement, (b) 0.5% n-SiO_2, (c) 1% n-SiO_2, (d) 1.5% n-SiO_2 and (e) 3% n-SiO_2 after being exposed to CO_2 saturated water for 56 days.

with reaction time square root (Abid et al., 2015; Bagheri et al., 2018; Bai et al., 2016; Kutchko et al., 2008). Comparing all cement systems from both 7 and 56 days, it can be observed that n-SiO_2 addition reduces portlandite depletion zone porosity, making the transition between carbonated and unreacted core smoother. Fig. 11 shows EDS line scan from two different cement systems with and without n-SiO_2 after being degraded by CO_2 for 56 days. Comparing the profiles and tendency line, the n-SiO_2 system exhibits a more homogeneous distribution of Ca and Si across carbonated zone and unreacted core. Therefore, in n-SiO_2 presence the CO_2 attack does not causes abrupt changes on chemical composition and microstructure, being favorable for properties and cement durability maintenance in such environment.

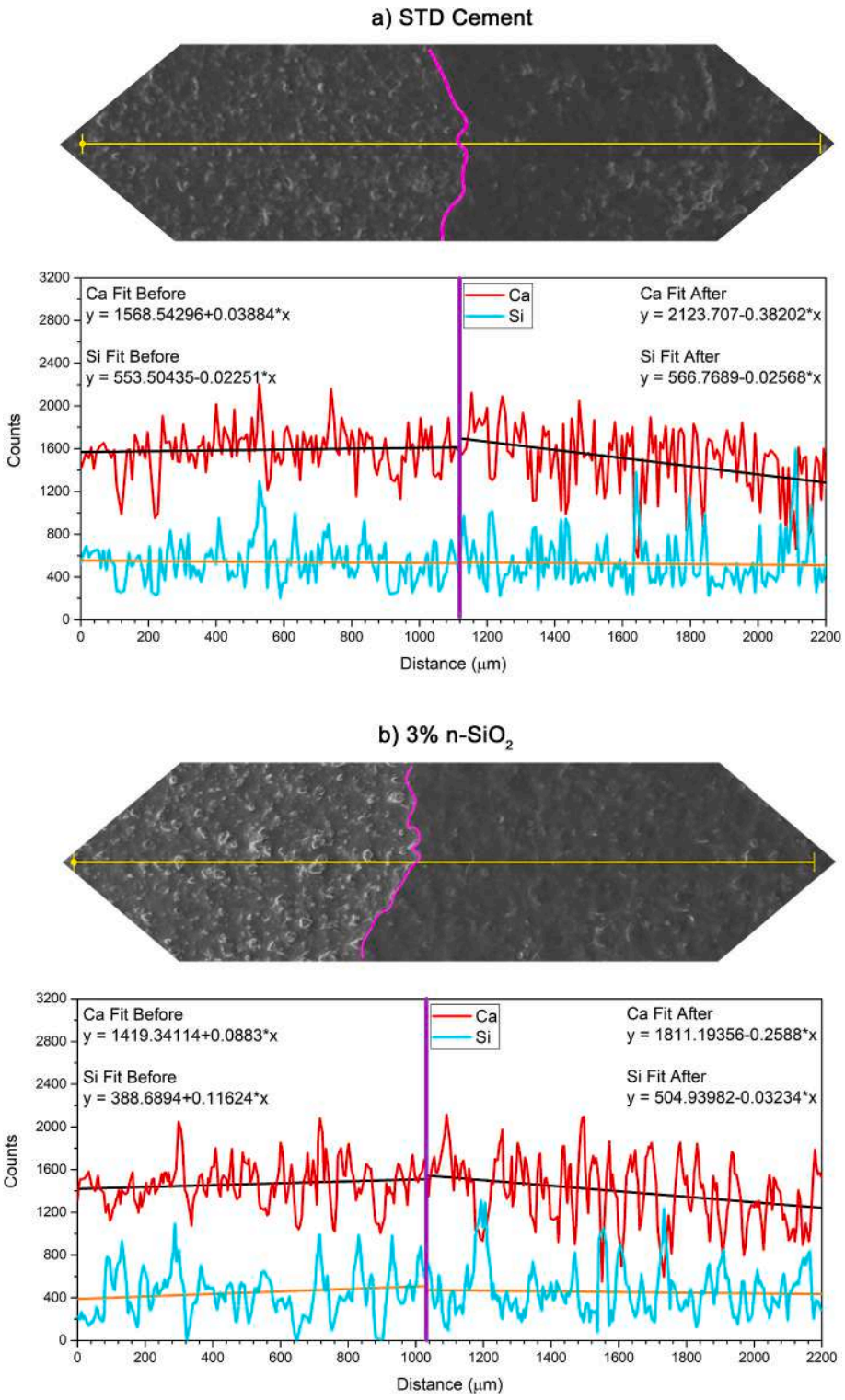

Fig. 11. Unreacted core-carbonated zone EDS line scan image from 3% n-SiO_3 after being exposed to CO_2-saturated water for 56 days.

Microtomography images in Fig. 12 also evidence differences in density in four zones: bicarbonated, carbonated, portlandite depletion and unreacted core. The carbonated zone is denser for 0.5% n-SiO_2 when compared to other cement systems, meeting the lowest degradation thickness value found for this particle amount. Furthermore, as the n-SiO_2 content increases, the transition between the zones become smoother, agreeing with SEM results of Fig. 8. The carbonation fronts are larger and less dense in n-SiO_2 presence.

The differences on the carbonated and portlandite depleted zones properties in the cement systems with and without n-SiO_2 are also evidenced in the AFM images, presented in Fig. 13. The STD cement system has a greater height variation than the system with n-SiO_2 addition. This means that the n-SiO_2 cement system presents a more compacted carbonated zone (lower roughness), indicating that the nucleation was increased by n-SiO_2 addition. This behavior was also observed by Feng et al. (2013) when incorporating TiO_2 nanoparticles in cement paste.

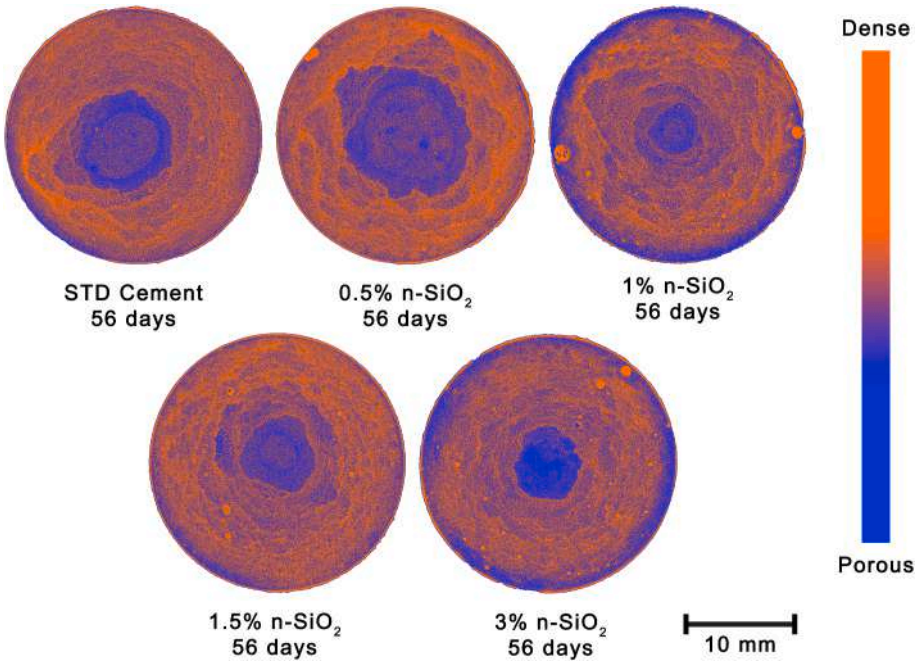

Fig. 12. Cement systems microtomography after being exposed to CO_2-saturated water for 56 days.

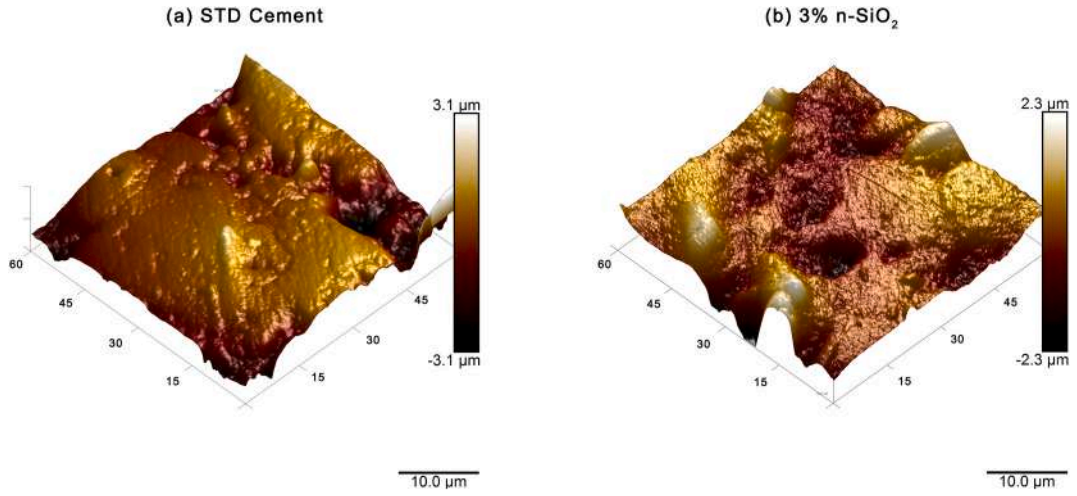

Fig. 13. AFM images from carbonated zone of (a) STD Cement and (b) 3% n-SiO_2 after being exposed to CO_2-saturated water for 56 days. The carbonation fronts are lighter and portlandite depleted zones are darker regions.

Table 5
Cement systems roughness after being exposed to CO_2-saturated water for 56 days.

Measurement locations	Cement Systems	
	STD Cement	3% n-SiO_2
Carbonated and portlandite depleted zones	774 nm	549 nm
Carbonated zone only	472 nm	265 nm

While in the STD cement the transition between carbonated fronts and depleted zone is narrow but deeper, in 3% n-SiO_2 the opposite occurs, the transition is larger but shallower. To quantify this difference, cement systems roughness was determined, and the results are presented in Table 5. STD cement presented a higher roughness when compared to 3% n-SiO_2 system, being this difference 41% when considering portlandite depleted zone and 78% when considering only carbonated zone.

Table 6
Cement systems Vickers microhardness average value after being exposed to CO_2-saturated water for 56 days.

Cement Systems	Bicarbonated zone (HV/0.05)	Carbonated zone (HV/0.05)	Unreacted core (HV/0.05)
STD Cement	56.92 ± 16.50	101.09 ± 42.71	75.97 ± 1.15
0.5% n-SiO_2	46.93 ± 12.02	109.67 ± 47.12	54.75 ± 9.15
1% n-SiO_2	43.31 ± 9.30	107.99 ± 44.45	64.60 ± 2.68
1.5% n-SiO_2	36.74 ± 11.44	117.39 ± 50.88	65.70 ± 6.12
3% n-SiO_2	42.38 ± 15.38	107.96 ± 46.73	74.07 ± 3.76

The AFM results are in agreement with microtomography and SEM images. Typically, a more uniform and denser microstructure is associated to a cement with enhanced mechanical properties and lower permeability.

Table 6 shows cement systems Vickers microhardness average

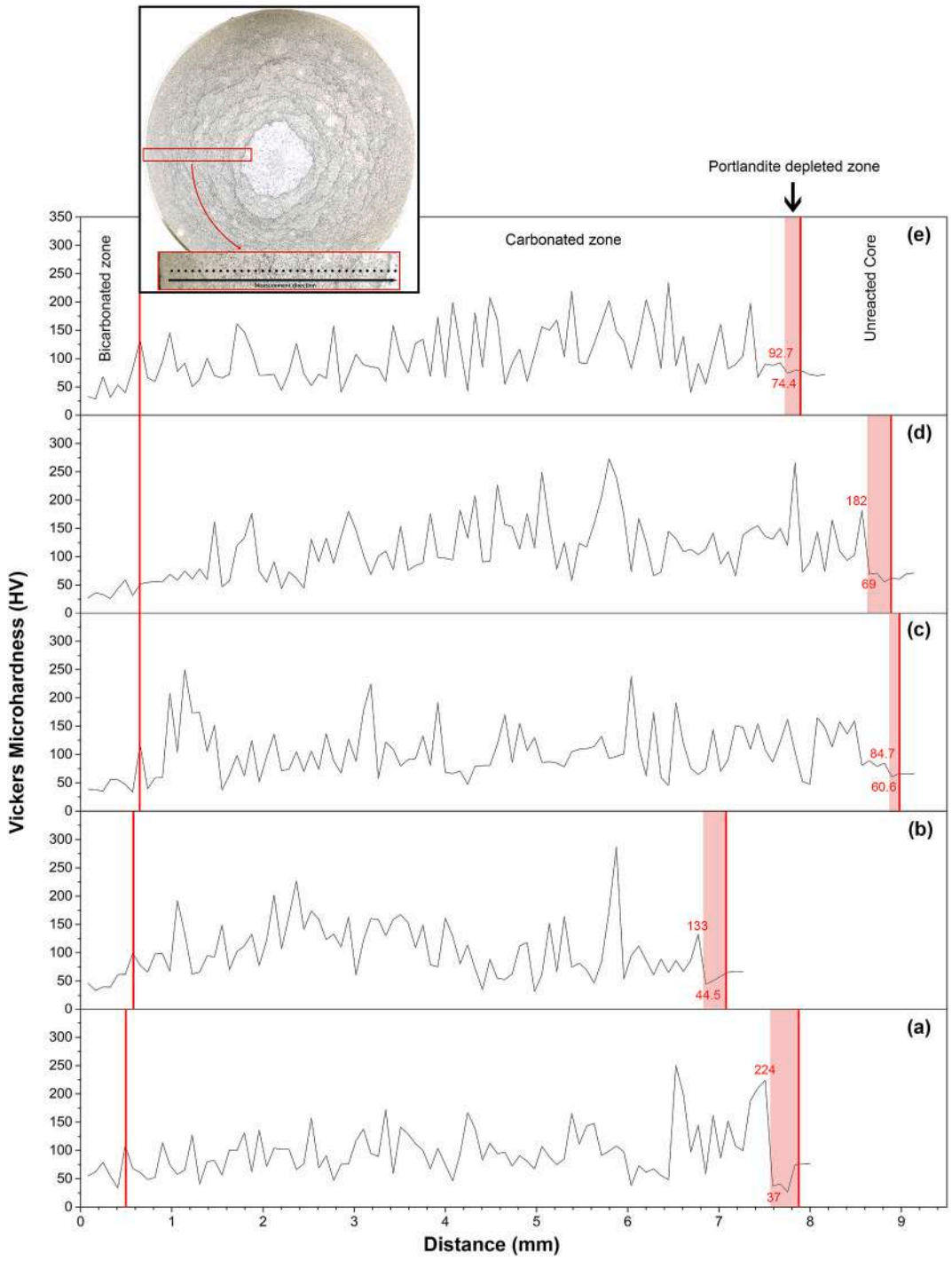

Fig. 14. Microhardness profile of (a) STD Cement (b) 0.5% n-SiO_2 (c) 1% n-SiO_2 (d) 1.5% n-SiO_2 and (e) 3% n-SiO_2 after being exposed to CO_2-saturated water for 56 days where the red lines represent the division of bicarbonated-carbonated zones and carbonated zone-unreacted core. (For interpretation of the references to colour in this figure legend, the reader is referred to the Web version of this article.)

values. Fig. 14 illustrates its profiles from the edge (bicarbonated zone) passing through carbonated and dissolution zone until reaching the unreacted core. The bicarbonated zone is rich in amorphous silica gel, and the material is very porous and weakened due to $CaCO_3$ dissolution, presenting a very low hardness. Carbonated zone has an increased hardness when compared with the unreacted core due to the pore space that is filled with $CaCO_3$. The hardness standard deviation is very high in the carbonated zone related to material heterogeneity due to the presence of multi carbonation fronts. The hardness behavior for the three zones of STD Cement system was similar to that observed by Kutchko et al. (2007). The authors found 25 HV for bicarbonate zone, 127.5 HV for carbonated zone and 64 HV for unaltered core, while we obtain about 57 HV, 102 HV and 76 HV, respectively.

Among all cement systems, STD Cement presented the higher hardness in bicarbonated zone, while the 1.5% n-SiO_2 system was 35.45% lower. On the other hand, the opposite occurs in the carbonated zone. 1.5% n-SiO_2 was the hardest system, with 117.39 HV and 13.89% higher than STD Cement. The systems with n-SiO_2 addition have a less hard bicarbonated zone, but a harder carbonated zone and core when compared to STD Cement. The drop on hardness in the portlandite

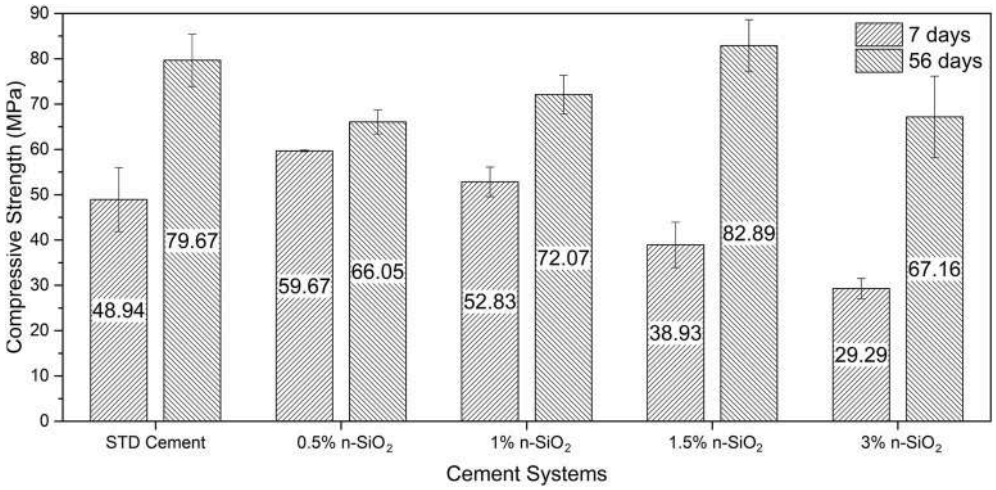

Fig. 15. Cement systems compressive strength before exposure to CO_2-saturated water for 7 and 56 days.

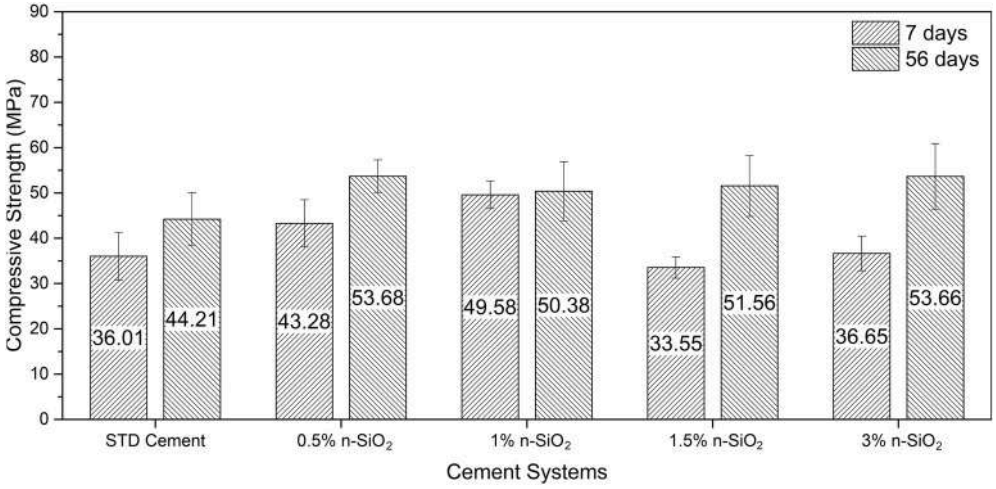

Fig. 16. Cement systems compressive strength after exposure to CO_2-saturated water for 7 and 56 days.

depleted zone (red zone in Fig. 14) is due to $Ca(OH)_2$ consumption to form $CaCO_3$, creating a porous and low mechanical properties region. The hardness decreasing in this zone was more pronounced in STD Cement and 0.5% n-SiO_2 cement system. In higher amounts of n-SiO_2 additions, this low hardness region is not significantly marked and also hardness transition is smoother along the whole profile. This is an advantageous effect of adding n-SiO_2 once it tends do not negatively impact the compressive strength, avoiding cracks formation in mechanical stress presence.

Fig. 15 and Fig. 16 present compressive strength results of cement systems from 7 to 56 days before and after being exposed to CO_2-saturated water, respectively. Unreacted STD Cement from 7 days demonstrated similar and even higher values to those also reported in literature for similar cement pastes with thermal curing (Barlet-Gouédard et al., 2007; Ge et al., 2018; Jeong et al., 2018; Mabeyo et al., 2020). At 7 days age the compressive strength is 48.94 MPa for STD Cement and increases to 79.67 MPa after 56 days associated to continuous hydration process.

The compressive strength before exposure to CO_2 reduces as more n-SiO_2 is added at 7 days age, from 59.67 MPa for 0.5% nSiO_2 to 29.29 MPa for 3% of n-SiO_2, as shown in Fig. 15. Compared with STD Cement the reduction on compressive strength for 3% of n-SiO_2 was about 40%. El-Gamal et al. (2017) observed a smaller decreasing on compressive strength from adding 1%–2% of n-SiO_2 for cement class G, but with a w/c ratio of 0.30 and cured at 90 °C for 7 days. However, at 56 age all unreacted n-SiO_2 cement systems presented high strength (from 66.05 MPa to 82.89 MPa) increasing with n-SiO_2 amount with exception of 3% n-SiO_2. One hypothesis why 3% n-SiO_2 presented lower compressive strength than 1.5% is probably due to particle agglomeration and uncompleted hydration, which needs to be further investigated.

After being exposed to CO_2 for earlier period (7 days), Fig. 16, the n-SiO_2 systems presented compressive strength in the range of 33.55 MPa–49.58 MPa, while STD Cement 36.01 MPa. 0.5 and 1% n-SiO_2 cement systems presented the higher compressive strength values corresponding to 20.19% and 38.29% superior than STD Cement, respectively. Comparison of the compressive strength decrease before and after exposition to CO_2 in 7 days showed similar values for the STD Cement and 0.5 n-SiO_2 systems (26.42% and 27.47% lower, respectively). However, the more n-SiO_2 addition reduced loss on the compressive strength and even increased as is the case of 3% n-SiO_2 system, showing an increment of 25.13%.

After being exposed to CO_2 for longer period (56 days), Fig. 16, all the n-SiO_2 cement systems performed better than STD Cement. Additionally, the n-SiO_2 amount had no expressive influence on the compressive strength, being the values between 50.38 MPa and 53.68 MPa. These values are in the range of 14%–21% higher than the STD Cement (44.21 MPa). Furthermore, the reduction of STD Cement compressive strength at 56 days due to CO_2 attack was 44.51%, while the loss on this property was reduced with the n-SiO_2 addition in all

cement systems. The minor reduction on compressive strength occurred in the 0.5% n-SiO_2 system (18.73%), while the loss increased in 1% and 1.5% of n-SiO_2 addition (30.10% and 37.80%). When 3% of n-SiO_2 is added, compressive strength loss is reduced to 20.10%.

Therefore, cement systems with n-SiO_2 addition demonstrated superior performance when compared to STD Cement, before and after being exposed to CO_2 at HPHT, particularly for long periods (56 days). This is probably related to n-SiO_2 pozzolanic and nanoparticles filler effect, increasing C–S–H production and matrix densification. In this aspect, adding n-SiO_2 is beneficial to improve the oil well cement performance against CO_2 under CCS condition.

4. Conclusions

Experimental research was used to investigate chemical and mechanical properties of cement paste containing SiO_2 nanoparticles after being exposed to CO_2-saturated water under CCS conditions. From the results reported in this paper the following conclusions can be drawn:

- The slurries workability decreased with n-SiO_2 addition because is smaller in particle size when compared to the cement, increasing solids surface area and the reactivity with water molecules to form chemical bonds.
- Although SiO_2 is less dense than cement, the hardened cement systems specific density measured by Helium pycnometry was not altered significantly in the n-SiO_2 presence. This is mainly because the cement quantity replaced by n-SiO_2 was very small and the nanoparticles filler effect.
- In all cement systems, with and without n-SiO_2, carbonation mechanism has been on multiple fronts. However, the n-SiO_2 influences on thickness, calcium and silicon content, density, roughness and hardness of the chemically altered layer. This is probably associated to the n-SiO_2 pozzolanic effect which is potentialized by the large n-SiO_2 particles surface area, reducing portlandite crystal size and amount, producing a more compact microstructure and enhancing cementitious matrix properties.
- The main advantage of n-SiO_2 adding in cement obtained is that the CO_2 attack does not causes abrupt changes on chemical composition, microstructure, density and hardness. This behavior was also confirmed by AFM images, where carbonation fronts were analyzed, and the roughness was measured. As a consequence, the compressive strength loss after reaction with CO_2 was lower in n-SiO_2 cement systems when compared to performance of STD Cement.
- The n-SiO_2 quantity which must be added to the cement to have the best performance varied with exposure time to CO_2. The 1.5% n-SiO_2 cement presented the lowest carbonation depth in early exposition time, while the 0.5% n-SiO_2 system performed better in long exposition time. After being exposed to CO_2 for longer period, the n-SiO_2 amount had no expressive influence on the compressive strength, and all the n-SiO_2 cement systems performed better than STD cement at HPHT.

CRediT authorship contribution statement

Giovanni dos Santos Batista: Conceptualization, Methodology, Validation, Formal analysis, Investigation, Data curation, Writing - original draft, Writing - review & editing, Visualization. **Luana Bottoli Schemmer:** Investigation, Visualization, Writing - original draft. **Tiago de Abreu Siqueira:** Investigation, Visualization, Writing - original draft. **Eleani Maria da Costa:** Conceptualization, Methodology, Validation, Formal analysis, Writing - original draft, Writing - review & editing, Supervision.

Declaration of competing interest

The authors declare that they have no known competing financial interests or personal relationships that could have appeared to influence the work reported in this paper.

Acknowledgements

This work was supported by the Institute of Petroleum and Natural Resources – IPR and The Unit Operations Laboratory – LOPE from PUCRS. This study was partly financed by the Coordenação de Aperfeiçoamento de Pessoal de Nível Superior – *Brasil* (CAPES) – Finance Code 001.

Appendix A. Supplementary data

Supplementary data to this article can be found online at https://doi.org/10.1016/j.petrol.2020.107742.

References

Abid, K., Gholami, R., Choate, P., Nagaratnam, B.H., 2015. A review on cement degradation under CO2-rich environment of sequestration projects. J. Nat. Gas Sci. Eng. 27, 1149–1157. https://doi.org/10.1016/j.jngse.2015.09.061.

Alawad, O.A., Alhozaimy, A., Jaafar, M.S., Aziz, F.N.A., Al-Negheimish, A., 2015. Effect of autoclave curing on the microstructure of blended cement mixture incorporating ground dune sand and ground granulated blast furnace slag. Int. J. Concr. Struct. Mater. 9, 381–390. https://doi.org/10.1007/s40069-015-0104-9.

Aminu, M.D., Nabavi, S.A., Rochelle, C.A., Manovic, V., 2017. A review of developments in carbon dioxide storage. Appl. Energy 208, 1389–1419. https://doi.org/10.1016/j.apenergy.2017.09.015.

Anwar, M.N., Fayyaz, A., Sohail, N.F., Khokhar, M.F., Baqar, M., Khan, W.D., Rasool, K., Rehan, M., Nizami, A.S., 2018. CO2 capture and storage: a way forward for sustainable environment. J. Environ. Manag. 226, 131–144. https://doi.org/10.1016/j.jenvman.2018.08.009.

API, 2009. 10A Specification for Cements and Materials for Well Cementing.

Bagheri, M., Shariatipour, S.M., Ganjian, E., 2018. A review of oil well cement alteration in CO2-rich environments. Construct. Build. Mater. 186, 946–968. https://doi.org/10.1016/j.conbuildmat.2018.07.250.

Bai, M., Sun, J., Song, K., Li, L., Qiao, Z., 2015. Well completion and integrity evaluation for CO2 injection wells. Renew. Sustain. Energy Rev. 45, 556–564. https://doi.org/10.1016/j.rser.2015.02.022.

Bai, M., Zhang, Z., Fu, X., 2016. A review on well integrity issues for CO 2 geological storage and enhanced gas recovery. Renew. Sustain. Energy Rev. 59, 920–926. https://doi.org/10.1016/j.rser.2016.01.043.

Barlet-Gouédard, V., Rimmelé, G., Goffé, B., Porcherie, O., 2007. Well technologies for CO 2 geological storage: CO 2 -resistant cement. Oil Gas Sci. Technol. - Rev. l'IFP 62, 325–334. https://doi.org/10.2516/ogst:2007027.

Barlet-Gouédard, V., Rimmelé, G., Porcherie, O., Quisel, N., Desroches, J., 2009. A solution against well cement degradation under CO2 geological storage environment. Int. J. Greenh. Gas Control 3, 206–216. https://doi.org/10.1016/j.ijggc.2008.07.005.

Bentz, D.P., 1997. Three-dimensional computer simulation of Portland cement hydration and microstructure development. J. Am. Ceram. Soc. 80, 19. https://doi.org/10.1111/j.1151-2916.1997.tb02785.x.

Bertos, M.F., Simons, S., Hills, C., Carey, P., 2004. A review of accelerated carbonation technology in the treatment of cement-based materials and sequestration of CO2. J. Hazard Mater. 112, 193–205. https://doi.org/10.1016/j.jhazmat.2004.04.019.

Bjørge, R., Gawel, K., Chavez Panduro, E.A., Torsæter, M., 2019. Carbonation of silica cement at high-temperature well conditions. Int. J. Greenh. Gas Control 82, 261–268. https://doi.org/10.1016/j.ijggc.2019.01.011.

Bu, Y., Hou, X., Wang, C., Du, J., 2018. Effect of colloidal nanosilica on early-age compressive strength of oil well cement stone at low temperature. Construct. Build. Mater. 171, 690–696. https://doi.org/10.1016/j.conbuildmat.2018.03.220.

Carey, W.J., Svec, R., Grigg, R., Zhang, J., Crow, W., 2010. Experimental investigation of wellbore integrity and CO2–brine flow along the casing–cement microannulus. Int. J. Greenh. Gas Control 4, 272–282. https://doi.org/10.1016/j.ijggc.2009.09.018.

Collins, F., Lambert, J., Duan, W.H., 2012. The influences of admixtures on the dispersion, workability, and strength of carbon nanotube–OPC paste mixtures. Cement Concr. Compos. 34, 201–207. https://doi.org/10.1016/j.cemconcomp.2011.09.013.

Duguid, A., Radonjic, M., Scherer, G.W., 2011. Degradation of cement at the reservoir/cement interface from exposure to carbonated brine. Int. J. Greenh. Gas Control 5, 1413–1428. https://doi.org/10.1016/j.ijggc.2011.06.007.

El-Diadamony, H., Amer, A.A., Sokkary, T.M., El-Hoseny, S., 2018. Hydration and characteristics of metakaolin pozzolanic cement pastes. HBRC J 14, 150–158. https://doi.org/10.1016/j.hbrcj.2015.05.005.

El-Gamal, S.M.A., Hashem, F.S., Amin, M.S., 2017. Influence of carbon nanotubes, nanosilica and nanometakaolin on some morphological-mechanical properties of oil well cement pastes subjected to elevated water curing temperature and regular room air curing temperature. Construct. Build. Mater. 146, 531–546. https://doi.org/10.1016/j.conbuildmat.2017.04.124.

Ershadi, V., Ebadi, T., Rabani, A., Ershadi, L., Soltanian, H., 2011. The effect of nanosilica on cement matrix permeability in oil well to decrease the pollution of receptive

environment. Int. J. Environ. Sustain Dev. 128–132. https://doi.org/10.7763/IJESD.2011.V2.109.
Feng, D., Xie, N., Gong, C., Leng, Z., Xiao, H., Li, H., Shi, X., 2013. Portland cement paste modified by TiO 2 nanoparticles: a microstructure perspective. Ind. Eng. Chem. Res. 52, 11575–11582. https://doi.org/10.1021/ie4011595.
Flores, Y.C., Cordeiro, G.C., Toledo Filho, R.D., Tavares, L.M., 2017. Performance of Portland cement pastes containing nano-silica and different types of silica. Construct. Build. Mater. 146, 524–530. https://doi.org/10.1016/j.conbuildmat.2017.04.069.
Ge, Z., Yao, X., Wang, X., Zhang, W., Yang, T., 2018. Thermal performance and microstructure of oil well cement paste containing subsphaeroidal konilite flour in HTHP conditions. Construct. Build. Mater. 172, 787–794. https://doi.org/10.1016/j.conbuildmat.2018.03.268.
Griffin, A.S., Rahman, M.K., Kim, J.J., Reda Taha, M., 2013. The significance of nanosilica on degradation of oil well cement in carbonated brine environments. In: Mechanics and Physics of Creep, Shrinkage, and Durability of Concrete. American Society of Civil Engineers, Reston, VA, pp. 372–379. https://doi.org/10.1061/9780784413111.044.
Hu, M., Guo, J., Li, P., Chen, D., Xu, Y., Feng, Y., Yu, Y., Zhang, H., 2019. Effect of characteristics of chemical combined of graphene oxide-nanosilica nanocomposite fillers on properties of cement-based materials. Construct. Build. Mater. 225, 745–753. https://doi.org/10.1016/j.conbuildmat.2019.07.079.
Huet, B., Tasoti, V., Khalfallah, I., 2011. A review of Portland cement carbonation mechanisms in CO2 rich environment. Energy Procedia 4, 5275–5282. https://doi.org/10.1016/j.egypro.2011.02.507.
Janković, K., Stanković, S., Bojović, D., Stojanović, M., Antić, L., 2016. The influence of nano-silica and barite aggregate on properties of ultra high performance concrete. Construct. Build. Mater. 126, 147–156. https://doi.org/10.1016/j.conbuildmat.2016.09.026.
Jeong, Y.J., Youm, K.S., Yun, T.S., 2018. Effect of nano-silica and curing conditions on the reaction rate of class G well cement exposed to geological CO2-sequestration conditions. Cement Concr. Res. 109, 208–216. https://doi.org/10.1016/j.cemconres.2018.05.001.
Kołakowski, K., De Preter, W., Van Gemert, D., Lamberts, L., Van Rickstal, F., 1994. Low shrinkage cement based building components. Cement Concr. Res. 24, 765–775. https://doi.org/10.1016/0008-8846(94)90202-X.
Kutchko, B.G., Strazisar, B.R., Dzombak, D.A., Lowry, G.V., Thaulow, N., 2007. Degradation of well cement by CO 2 under geologic sequestration conditions. Environ. Sci. Technol. 41, 4787–4792. https://doi.org/10.1021/es062828c.
Kutchko, B.G., Strazisar, B.R., Huerta, N., Lowry, G.V., Dzombak, D.A., Thaulow, N., 2009. CO 2 reaction with hydrated class H well cement under geologic sequestration conditions: effects of flyash admixtures. Environ. Sci. Technol. 43, 3947–3952. https://doi.org/10.1021/es803007e.
Kutchko, B.G., Strazisar, B.R., Lowry, G.V., Dzombak, D.A., Thaulow, N., 2008. Rate of CO 2 attack on hydrated class H well cement under geologic sequestration conditions. Environ. Sci. Technol. 42, 6237–6242. https://doi.org/10.1021/es800049r.
Lake, Larry W., Lotfollahi, Mohammad, Bryant, Steven L., 2019. Chapter 2 - CO_2 Enhanced Oil Recovery Experience and its Messages for CO_2 Storage. Science of Carbon Storage in Deep Saline Formations. Elsevier. https://doi.org/10.1016/C2016-0-03237-0.
Lavergne, F., Belhadi, R., Carriat, J., Ben Fraj, A., 2019. Effect of nano-silica particles on the hydration, the rheology and the strength development of a blended cement paste. Cement Concr. Compos. 95, 42–55. https://doi.org/10.1016/j.cemconcomp.2018.10.007.
Ledesma, R.B., Lopes, N.F., Bacca, K.G., Moraes, M.K. de, Batista, G., dos, S., Pires, M.R., Costa, E.M. da, 2020. Zeolite and fly ash in the composition of oil well cement: evaluation of degradation by CO2 under geological storage condition. J. Petrol. Sci. Eng. 185, 106656. https://doi.org/10.1016/j.petrol.2019.106656.
Lesti, M., Tiemeyer, C., Plank, J., 2013. CO2 stability of Portland cement based well cementing systems for use on carbon capture & storage (CCS) wells. Cement Concr. Res. 45, 45–54. https://doi.org/10.1016/j.cemconres.2012.12.001.
Leung, D.Y.C., Caramanna, G., Maroto-Valer, M.M., 2014. An overview of current status of carbon dioxide capture and storage technologies. Renew. Sustain. Energy Rev. 39, 426–443. https://doi.org/10.1016/j.rser.2014.07.093.
Liu, H.H., Yu, Y., Liu, H.H., Jin, J., Liu, S., 2018. Hybrid effects of nano-silica and graphene oxide on mechanical properties and hydration products of oil well cement. Construct. Build. Mater. 191, 311–319. https://doi.org/10.1016/j.conbuildmat.2018.10.029.
Mabeyo, P.E., Ibrahim, Y.S., Gu, J., 2020. Effect of high metakaolin content on compressive and shear-bond strengths of oil well cement at 80 °C. Construct. Build. Mater. 240, 117962. https://doi.org/10.1016/j.conbuildmat.2019.117962.
Marshdi, Q.S.R., 2018. Benefits of using mineral additives, as components of the modern oil-well cement. Case Stud. Constr. Mater. 8, 455–458. https://doi.org/10.1016/j.cscm.2018.03.010.
Matteo, E.N., Huet, B., Jové-Colón, C.F., Scherer, G.W., 2018. Experimental and modeling study of calcium carbonate precipitation and its effects on the degradation of oil well cement during carbonated brine exposure. Cement Concr. Res. 113, 1–12. https://doi.org/10.1016/j.cemconres.2018.03.016.
Mehta, P.K., Monteiro, P.J.M., 2013. Concrete: Microstructure, Properties and Materials, fourth. McGraw Hill Professional, Berkeley.
Murthy, R.V.V.R., Chavali, M., Mohammad, F., 2019. Synergistic effect of nano-silica slurries for cementing oil and gas wells. Pet. Res. https://doi.org/10.1016/j.ptlrs.2019.10.001.
Nawy, E.G., 2008. Concrete Construction Engineering Handbook, second ed. CRC Press, New York.
Nelson, E.B., Guillot, D., 2006. Well Cementing, second ed. Schlumberger, Texas.
Neville, A.M., 2018. Properties of Concrete, Fifth. ed. Pearson Education Limited, Harlow, United Kingdom.
Omosebi, O., Maheshwari, H., Ahmed, R., Shah, S., Osisanya, S., Hassani, S., DeBruijn, G., Cornell, W., Simon, D., 2016. Degradation of well cement in HPHT acidic environment: effects of CO2 concentration and pressure. Cement Concr. Compos. 74, 54–70. https://doi.org/10.1016/j.cemconcomp.2016.09.006.
Pang, X., Cuello Jimenez, W., Iverson, B.J., 2013. Hydration kinetics modeling of the effect of curing temperature and pressure on the heat evolution of oil well cement. Cement Concr. Res. 54, 69–76. https://doi.org/10.1016/j.cemconres.2013.08.014.
Paul, S.C., van Rooyen, A.S., van Zijl, G.P.A.G., Petrik, L.F., 2018. Properties of cement-based composites using nanoparticles: a comprehensive review. Construct. Build. Mater. 189, 1019–1034. https://doi.org/10.1016/j.conbuildmat.2018.09.062.
Rostami, M.R., Abbassi-Sourki, F., Bouhendi, H., 2019. Synergistic effect of branched polymer/nano silica on the microstructures of cement paste and their rheological behaviors. Construct. Build. Mater. 201, 159–170. https://doi.org/10.1016/j.conbuildmat.2018.12.103.
Santra, A.K., Boul, P., Pang, X., 2012. Influence of nanomaterials in oilwell cement hydration and mechanical properties. In: SPE International Oilfield Nanotechnology Conference and Exhibition. Society of Petroleum Engineers. https://doi.org/10.2118/156937-MS.
Senff, L., Labrincha, J.A., Ferreira, V.M., Hotza, D., Repette, W.L., 2009. Effect of nano-silica on rheology and fresh properties of cement pastes and mortars. Construct. Build. Mater. 23, 2487–2491. https://doi.org/10.1016/j.conbuildmat.2009.02.005.
Shao, J., Gao, J., Zhao, Y., Chen, X., 2019. Study on the pozzolanic reaction of clay brick powder in blended cement pastes. Construct. Build. Mater. 213, 209–215. https://doi.org/10.1016/j.conbuildmat.2019.03.307.
Soares, L.W.O., Braga, R.M., Freitas, J.C.O., Ventura, R.A., Pereira, D.S.S., Melo, D.M.A., 2015. The effect of rice husk ash as pozzolan in addition to cement Portland class G for oil well cementing. J. Petrol. Sci. Eng. 131, 80–85. https://doi.org/10.1016/j.petrol.2015.04.009.
Taylor, H.F.W., 1990. Cement Chemistry. Academic Press, London.
Thakkar, A., Raval, A., Chandra, S., Shah, M., Sircar, A., 2019. A comprehensive review of the application of nano-silica in oil well cementing. Petroleum. https://doi.org/10.1016/j.petlm.2019.06.005.
van der Meer, B., 2005. Carbon dioxide storage in natural gas reservoirs. Oil Gas Sci. Technol. 60, 527–536.
Wang, T., Ishida, T., 2019. Multiphase pozzolanic reaction model of low-calcium fly ash in cement systems. Cement Concr. Res. 122, 274–287. https://doi.org/10.1016/j.cemconres.2019.04.015.
Xiao, H., Zhang, F., Liu, R., Zhang, R., Liu, Z., Liu, H., 2019. Effects of pozzolanic and non-pozzolanic nanomaterials on cement-based materials. Construct. Build. Mater. 213, 1–9. https://doi.org/10.1016/j.conbuildmat.2019.04.057.
Yan, J., Zhang, Z., 2019. Carbon capture, utilization and storage (CCUS). Appl. Energy 235, 1289–1299. https://doi.org/10.1016/j.apenergy.2018.11.019.
Yang, Y., Yuan, B., Wang, Y., Zhang, S., Zhu, L., 2016. Carbonation resistance cement for CO 2 storage and injection wells. J. Petrol. Sci. Eng. 146, 883–889. https://doi.org/10.1016/j.petrol.2016.08.006.
Zhang, L., Dzombak, D.A., Nakles, D.V., Hawthorne, S.B., Miller, D.J., Kutchko, B.G., Lopano, C.L., Strazisar, B.R., 2014. Rate of H2S and CO2 attack on pozzolan-amended Class H well cement under geologic sequestration conditions. Int. J. Greenh. Gas Control 27, 299–308. https://doi.org/10.1016/j.ijggc.2014.02.013.
Zhang, L., Dzombak, D.A., Nakles, D.V., Hawthorne, S.B., Miller, D.J., Kutchko, B.G., Lopano, C.L., Strazisar, B.R., 2013. Characterization of pozzolan-amended wellbore cement exposed to CO2 and H2S gas mixtures under geologic carbon storage conditions. Int. J. Greenh. Gas Control 19, 358–368. https://doi.org/10.1016/j.ijggc.2013.09.004.
Zhang, M., Bachu, S., 2011. Review of integrity of existing wells in relation to CO2 geological storage: what do we know? Int. J. Greenh. Gas Control 5, 826–840. https://doi.org/10.1016/j.ijggc.2010.11.006.
Zhang, M., Talman, S., 2014. Experimental study of well cement carbonation under geological storage conditions. Energy Procedia 63, 5813–5821. https://doi.org/10.1016/j.egypro.2014.11.614.
Zhuang, C., Chen, Y., 2019. The effect of nano-SiO2 on concrete properties: a review. Nanotechnol. Rev. 8, 562–572. https://doi.org/10.1515/ntrev-2019-0050.